

Strengthening of the Walker Circulation under Global Warming in an Aqua-Planet General Circulation Model Simulation

Tim LI^{1,2}, ZHANG Lei^{*1}, and Hiroyuki MURAKAMI³

¹*AORC/IPRC and Department of Atmospheric Sciences, University of Hawaii, 2525 Correa Rd., Honolulu HI 96822, USA*

²*International Laboratory on Climate and Environment Change and Key Laboratory of Meteorological Disaster,*

Nanjing University of Information Science and Technology, Nanjing 210044

³*Climate Research Department, Meteorological Research Institute, Tsukuboda, Ibaraki 305-0052, Japan*

(Received 30 January 2015; revised 27 April 2015; accepted 27 May 2015)

ABSTRACT

Most climate models project a weakening of the Walker circulation under global warming scenarios. It is argued, based on a global averaged moisture budget, that this weakening can be attributed to a slower rate of rainfall increase compared to that of moisture increase, which leads to a decrease in ascending motion. Through an idealized aqua-planet simulation in which a zonal wavenumber-1 SST distribution is prescribed along the equator, we find that the Walker circulation is strengthened under a uniform 2-K SST warming, even though the global mean rainfall–moisture relationship remains the same. Further diagnosis shows that the ascending branch of the Walker cell is enhanced in the upper troposphere but weakened in the lower troposphere. As a result, a “double-cell” circulation change pattern with a clockwise (anti-clockwise) circulation anomaly in the upper (lower) troposphere forms, and the upper tropospheric circulation change dominates. The mechanism for the formation of the “double cell” circulation pattern is attributed to a larger (smaller) rate of increase of diabatic heating than static stability in the upper (lower) troposphere. The result indicates that the future change of the Walker circulation cannot simply be interpreted based on a global mean moisture budget argument.

Key words: Walker circulation, global warming, aqua-planet simulation

Citation: Li, T., L. Zhang, and H. Murakami, 2015: Strengthening of the Walker circulation under global warming in an aqua-planet general circulation model simulation. *Adv. Atmos. Sci.*, **32**(11), 1473–1480, doi: 10.1007/s00376-015-5033-7.

1. Introduction

Considerable debate exists among climate scientists as to how the tropical Walker circulation and sea surface temperature (SST) pattern will change due to the emissions of greenhouse gases under the influence of anthropogenic activities (Knutson and Manabe, 1995; Clement et al., 1996; Held and Soden, 2006; Vecchi et al., 2006, 2008; IPCC, 2007, 2013; Vecchi and Soden, 2007; Dinezio et al., 2009, 2010; Schneider et al., 2010; Merrifield, 2011; Bayr et al., 2014; Sandeep et al., 2014). Clement et al. (1996) suggested, from a purely oceanographic point of view, that a La Niña-like SST pattern with a strengthened Walker circulation will occur under global warming due to the increase of upper-ocean stratification. Held and Soden (2006) argued, from a global atmospheric moisture budget point of view, that because global mean precipitation increases at a smaller rate (around 1%–2% per 1 K of warming) than that of moisture (around 6%–7% per 1 K of warming), the global mean mass flux or ascending

motion must decrease in the future warmer state. The cause of the rainfall–moisture “mismatch” is attributed to the global atmospheric energy balance constraint that precipitation or latent heating increase is to a large extent balanced by the change of radiative cooling, which depends on the square root of moisture in the air column (Shine et al., 1990). A recent theoretical study suggests that an El Niño-like warming or a weakening of the Walker cell is primarily determined by the current climate mean state through a longwave radiative–evaporative damping mechanism (Zhang and Li, 2014).

In the tropics, due to the weak horizontal temperature gradient, atmospheric adiabatic cooling associated with ascending motion is approximately balanced by diabatic heating in either present-day (PD) or global warming (GW) climate states. The anthropogenic forcing may induce two competing processes in changing vertical motion. On the one hand, SST warming causes an increase of lower-tropospheric moisture, which can strengthen ascending motion through enhanced diabatic heating. On the other hand, upper-tropospheric temperature increases at a higher rate than lower-tropospheric temperature and, as a result, the atmosphere becomes more stable, which leads to the decrease of ascending motion

* Corresponding author: ZHANG Lei
Email: zhanglei@hawaii.edu

(Knutson and Manabe, 1995). Thus, the change of the ascending branch of the Walker circulation would depend on the relative importance of these two competing processes.

The motivation behind the present study is based on the observational analysis results reported by Hsu and Li (2012), who found there is competition between the monsoon and surrounding circulation systems (such as the intertropical convergence zones over the equatorial Indian Ocean in boreal summer and over the Atlantic in boreal winter) under global warming, and that only “the richest becomes richer”. It is also motivated by the fact that land surface warming is much greater than ocean warming under global warming. To eliminate the monsoon and land impacts and examine the “pure” Walker circulation response to global warming, we design a set of idealized numerical experiments in an aqua-planet Earth. Through diagnosis of the idealized simulation outputs, we hope to understand the relative importance of the moisture effect versus the stability effect in affecting the Walker circulation strength.

2. Idealized model setting

We consider an idealized water-covered Earth in which there is no monsoon or excessive land warming effect. A zonal wavenumber-1 zonal SST distribution is specified in the tropics (within 20°S–20°N). The model used for this study is an atmospheric general circulation model developed at the Japan Meteorological Agency Meteorological Research Institute (MRI). For a detailed description of this model, readers are referred to Yukimoto et al. (2011) and Mizuta et al. (2012). The model resolution is T106, and each simulation is integrated for 10 years. Solar radiation in this idealized experiment is fixed at the equinox.

Figure 1 shows the idealized SST pattern in the PD climate state. The SST is symmetric about the equator, with maximum amplitude directly on the equator. Along the equator, the highest (lowest) SST is located at 120°E (60°W). In

the GW climate state, a global uniform 2-K warming is imposed and the CO₂ concentration is doubled.

One of the greatest uncertainties in future projections by climate models is cumulus parameterization (e.g., Stocker, 2001). To test the sensitivity of the simulation results to the model convective parameterization scheme, three parallel runs with the Yoshimura et al. (2015) (hereafter YS), Arakawa and Schubert (1974) (hereafter AS) and Kain and Fritsch (1990, 1993) (hereafter KF) convective parameterization schemes have been carried out for both the PD and GW climate simulations. It has been shown that the MRI model with these schemes can simulate realistic climatological mean states of tropical and monsoon precipitation (Endo et al., 2012) and realistic tropical cyclone distributions (Murakami et al., 2012).

3. Results

In the presence of an idealized zonal wavenumber-1 SST distribution, the Walker circulation is well simulated in both the PD and GW states (Fig. 2). Maximum ascending motion and precipitation appear over the warmest pool, and minimum rainfall and descending motion appear around 60°W. The most striking difference between the GW and PD simulations lies in the change of the vertical motion profile over the ascending branch of the Walker circulation around 120°E (Fig. 2c). The ascending motion is strengthened (weakened) in the upper (lower) troposphere. Consistent with the vertical velocity change, a westerly anomaly appears in the upper and lower levels, while an easterly anomaly appears between (Fig. 2c). As a result, an anomalous “double-cell” vertical overturning circulation pattern with a clockwise (counterclockwise) cell in the upper (lower) troposphere forms. The separation line between the upper and lower cells appears at 300 hPa. Figure 3 further confirms that the “double-cell” pattern is a robust signal that can be found in each individual experiment with different convective parameterization schemes.

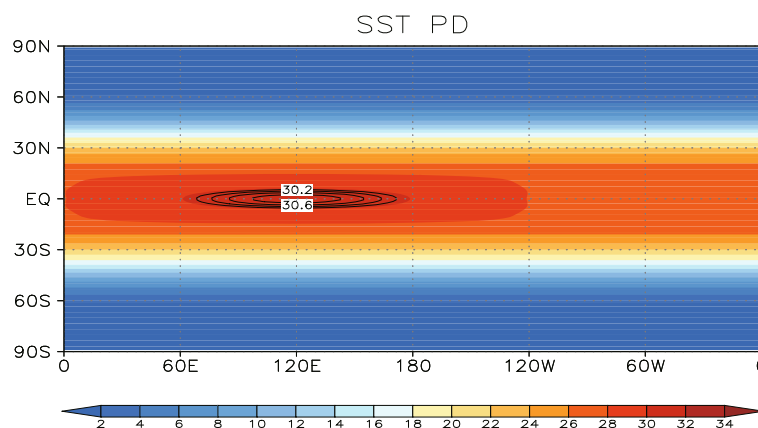


Fig. 1. Horizontal pattern of a prescribed SST field in the PD simulation. The SST field is symmetric about the equator (units: °C). It peaks at the equator and decreases poleward. Along the equator, the highest SST (31°C) is located at 120°E and the lowest SST (27°C) is located at 60°W.

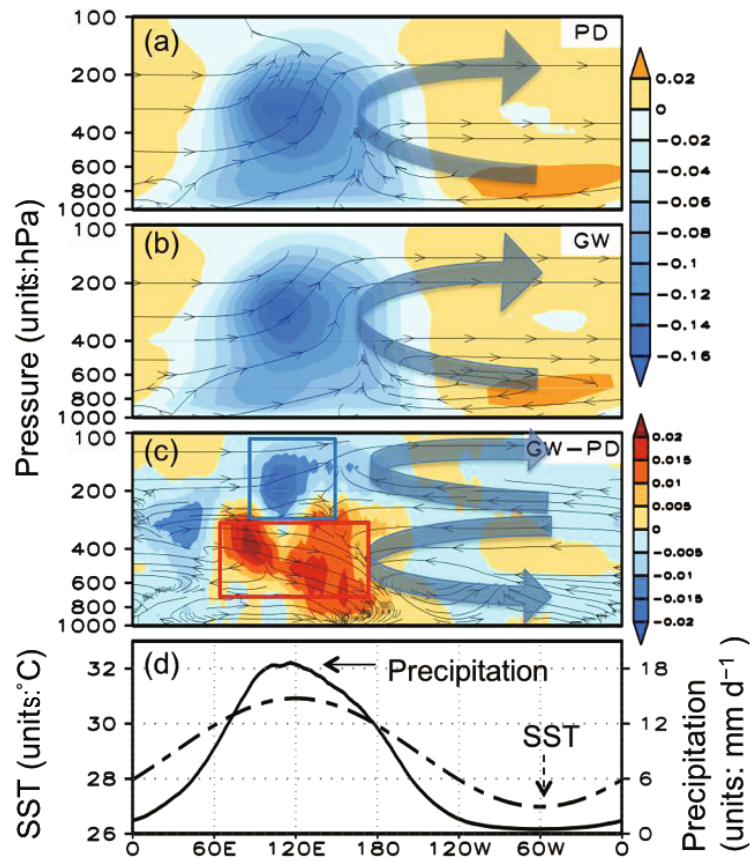


Fig. 2. Zonal-vertical cross sections of zonal overturning circulation (vectors) and vertical p -velocity (color scale; units: Pa s^{-1}) averaged between 2°S and 2°N , derived from the ensemble average of the YS, AS and KF simulations: (a) PD simulation; (b) GW simulation; (c) GW minus PD. (d) Zonal distribution of SST (dashed; unit: $^{\circ}\text{C}$) and precipitation (solid; units: mm d^{-1}) in the PD simulation.

An important issue is how to quantitatively measure the change of the strength of the Walker circulation. The area-averaged change of vertical motion at the ascending branch of the Walker circulation is plotted in Fig. 4a. The ascending motion is strengthened above 300 hPa but weakened below 300 hPa, and remains unchanged at the maximum vertical velocity level (300 hPa). Thus, the vertical motion over the region cannot be used to determine the change in overall strength of the Walker circulation. In previous studies (e.g., Vecchi et al., 2006), the difference of sea-level pressure (SLP) between the Western and Eastern Hemisphere was used to measure the strength of the Walker circulation. However, as shown in Fig. 5 and Table 1, such a definition is highly sensitive to the domain selected in the idealized aqua-planet simulations. For example, the change of the east-west SLP gradient is negative when the domains $60^{\circ}\text{--}0^{\circ}\text{W}$ and $120^{\circ}\text{--}180^{\circ}\text{E}$ are used, but becomes positive when the domains $70^{\circ}\text{--}0^{\circ}\text{W}$ and $110^{\circ}\text{--}180^{\circ}\text{E}$ (in which the domains are only expanded westward by 10° longitude) are used (Table 1). This suggests that the zonal SLP gradient (which mainly measures low-level zonal wind) is also not a good indicator.

Table 1. (a) The SLP differences between $60^{\circ}\text{--}0^{\circ}\text{W}$ and $120^{\circ}\text{--}180^{\circ}\text{E}$ averaged over three latitudinal bands in the PD and GW simulations and their difference (units: Pa). (b) As in (a) but for the SLP differences between $70^{\circ}\text{--}0^{\circ}\text{W}$ and $110^{\circ}\text{--}180^{\circ}\text{E}$.

(a)	SLP difference (Pa)		
	PD	GW	(GW-PD)
$0.5^{\circ}\text{S}\text{--}0.5^{\circ}\text{N}$	446.295	444.078	-2.217
$2^{\circ}\text{N}\text{--}2^{\circ}\text{S}$	446.411	444.207	-2.204
$5^{\circ}\text{N}\text{--}5^{\circ}\text{S}$	445.952	443.947	-2.005
(b)	SLP difference (Pa)		
	PD	GW	(GW-PD)
$0.5^{\circ}\text{S}\text{--}0.5^{\circ}\text{N}$	428.057	428.726	0.669
$2^{\circ}\text{N}\text{--}2^{\circ}\text{S}$	428.3	429.05	0.75
$5^{\circ}\text{N}\text{--}5^{\circ}\text{S}$	428.223	429.237	1.014

Given the great uncertainty in both the SLP and vertical motion fields, we decide to use the original definition of circulation (Holton, 2004) to measure the strength of the Walker circulation. The strength of zonal overturning circulation in

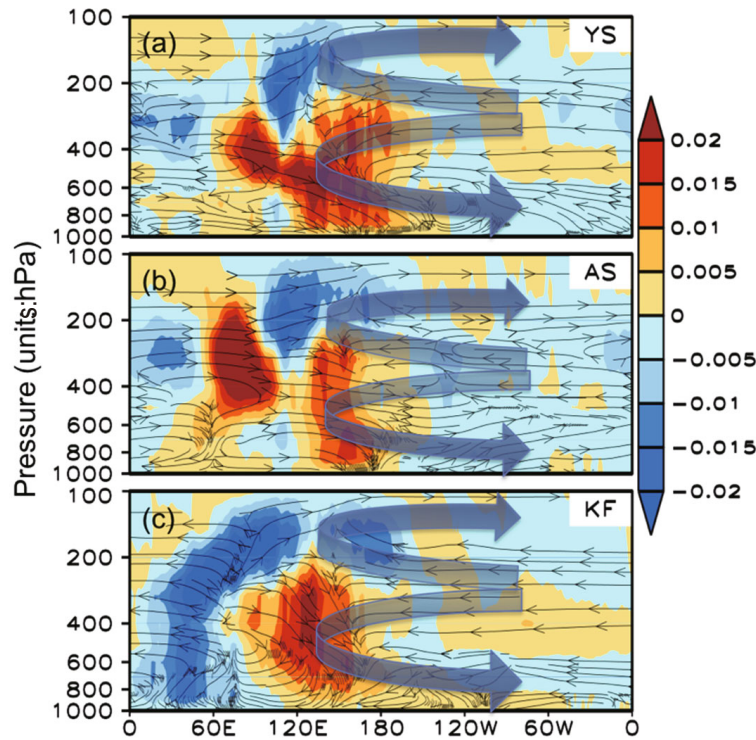


Fig. 3. Zonal–vertical cross sections of zonal overturning circulation (vectors) and vertical p -velocity (color scale; units: Pa s^{-1}) averaged between 2°S and 2°N in the (a) YS, (b) AS and (c) KF simulations, respectively.

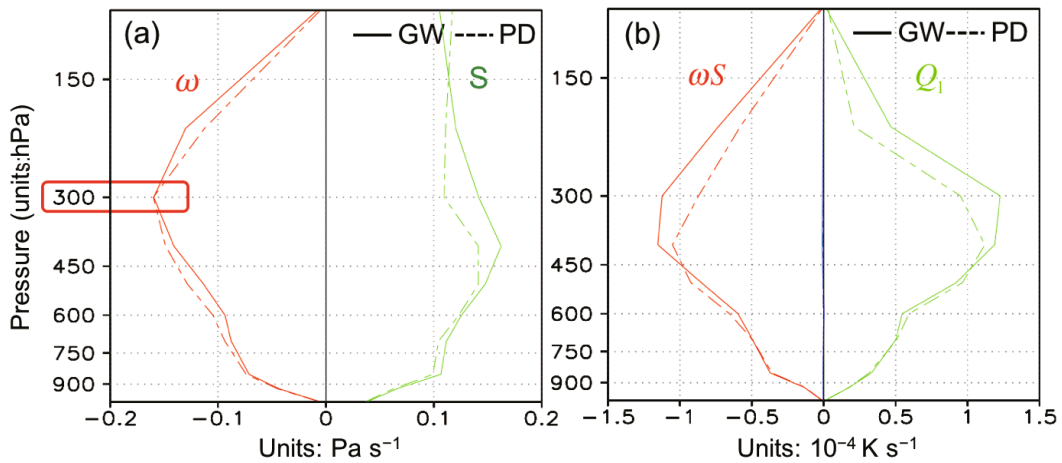


Fig. 4. (a) The vertical profile of p -velocity (red; units: Pa s^{-1}) and static stability (green; units: 0.5 K hPa^{-1}) averaged over $110^\circ\text{--}130^\circ\text{E}$ and $2^\circ\text{S--}2^\circ\text{N}$. (b) The vertical profile of Q_1 (green; units: 10^{-4} K s^{-1}), horizontal temperature advection (blue; units: 10^{-4} K s^{-1}) and adiabatic heating (red; units: 10^{-4} K s^{-1}) averaged over $110^\circ\text{--}130^\circ\text{E}$ and $2^\circ\text{S--}2^\circ\text{N}$. In both panels, the vertical profiles are derived from the ensemble average of the YS, AS and KF simulations. The solid line denotes GW and the dashed line PD.

the longitude–height cross section may be calculated according to an area integral of meridional vorticity

$$\iint \left(\frac{1}{\rho^2 g^2} \frac{\partial \omega}{\partial x} - \frac{\partial u}{\partial p} \right) dx dp,$$

where ω is vertical p -velocity (ω). This circulation definition contains the combined information of both the vertical motion and the zonal wind in a large longitude–height

domain. Figure 6 shows that the climatological maximum westerly (easterly) wind locates at 150 hPa (925 hPa) in both the PD and GW simulations, while the strongest upward motion appears near 120°E . Considering a longitude–height domain of $120^\circ\text{E--}60^\circ\text{W}$ and 925–150 hPa, we calculate the percentage change of the intensity of the Walker circulation in the PD and GW simulations averaged over three latitudinal zones (Table 2). The results show that the Walker circula-

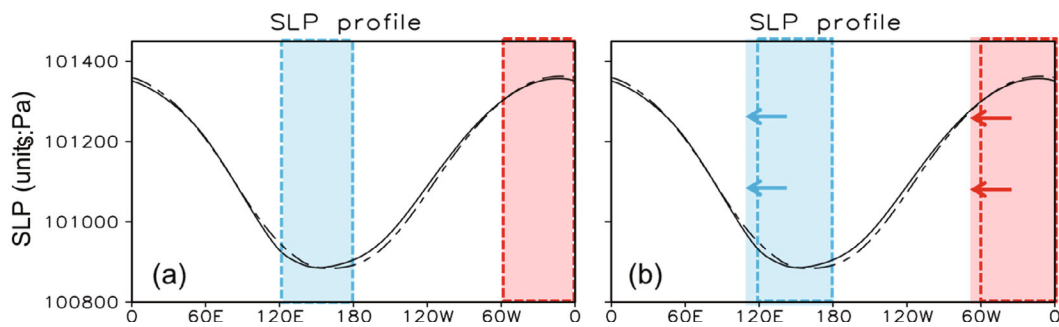


Fig. 5. The SLP profiles averaged from 2°S to 2°N derived from the ensemble average of the YS, AS and KF simulations (unit: Pa). The solid (dashed) line denotes the GW (PD) simulation. The red shading in (a) represents the region between 60°W and 0°W, and the blue between 120°E and 180°E. In (b), the red shading represent the region between 70°W and 0°W, and blue between 110°E and 180°E.

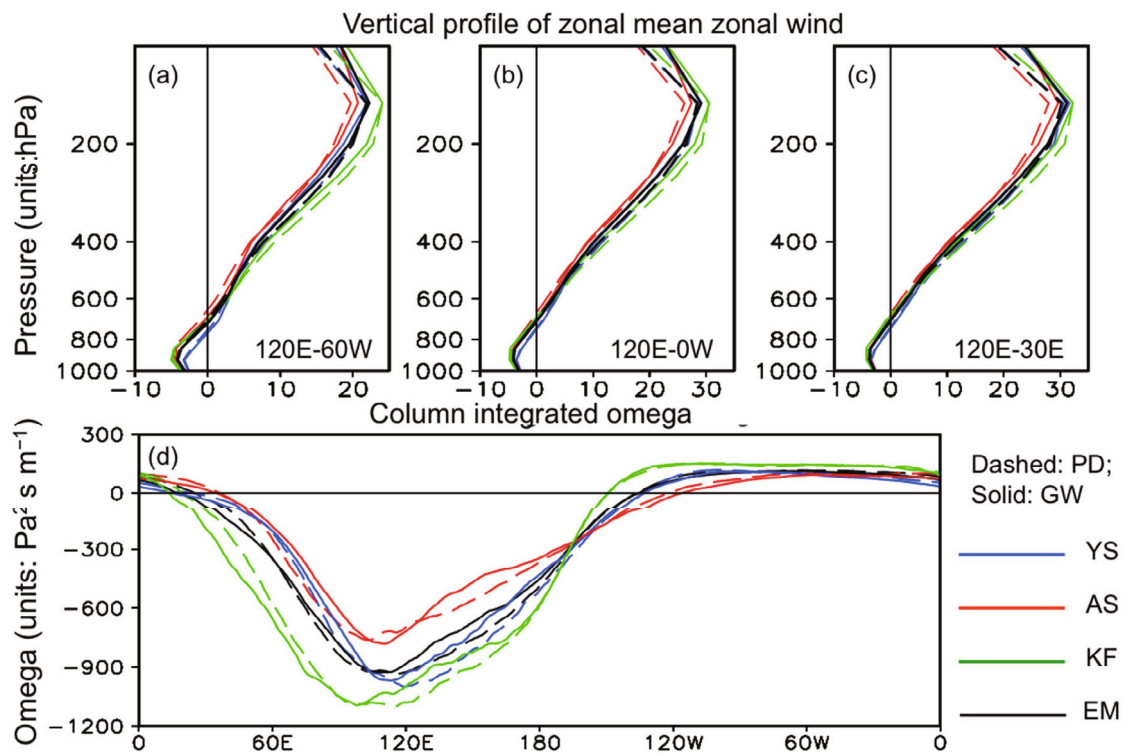


Fig. 6. Vertical profiles of zonal mean zonal wind (units: $m s^{-1}$) averaged in (a) 120°E–60°W, (b) 120°E–0°W and (c) 120°E–30°E. (d) Mass weighted column-integrated omega (units: $Pa^2 s m^{-1}$) averaged between 2°N and 2°S. The solid (dashed) curve is for the GW (PD) simulation (blue for the YS, red for the AS and green for the KF experiment).

tion is strengthened under global warming in all three convective parameterization sensitivity experiments, regardless of the latitudinal band chosen. We further test the sensitivity of the result to the longitudinal domain. Given that the Kelvin wave response length scale (in response to a given heating in the warm pool) is greater than the Rossby wave response length scale, additional calculations with greater longitudinal domains, 120°E–0°W and 120°E–30°E, are performed (Table 2). In the latter case, the Kelvin wave response length scale (270°) is exactly three times as large as the Rossby wave response length scale (90°). The result indicates that the Walker circulation strengthening signal is robust.

Since the change of zonal overturning circulation in the equatorial plane exhibits a “double-cell” pattern, with clockwise (counter-clockwise) circulation change in the upper (lower) troposphere (Figs. 2 and 3), we further examine which cell dominates the overall strength of the Walker circulation. Our calculation shows that the change of strength of the Walker circulation in the idealized aqua-planet model is primarily controlled by the upper cell circulation change. But what causes the strengthening of the upper-tropospheric vertical motion? In the tropics, where the horizontal temperature gradient is small, for both the PD and GW equilibrium state, the adiabatic cooling associated with vertical motion is

Table 2. The percentage change (GW – PD/PD) of intensity of the Walker circulation (units: %) calculated based on the original definition of circulation in different longitude–latitude domains and from 925 hPa to 150 hPa. The results are derived from the ensemble average of the YS, AS and KF simulations.

(a)	SLP difference (Pa)		
	PD	GW	(GW–PD)
0.5°S–0.5°N	446.295	444.078	–2.217
2°N–2°S	446.411	444.207	–2.204
5°N–5°S	445.952	443.947	–2.005
(b)	SLP difference (Pa)		
	PD	GW	(GW–PD)
0.5°S–0.5°N	428.057	428.726	0.669
2°N–2°S	428.3	429.05	0.75
5°N–5°S	428.223	429.237	1.014

approximately in balance with the diabatic heating term; thus,

$$\omega S + Q_1 = 0. \quad (1)$$

In Eq. (1), S denotes atmospheric static stability and Q_1 represents apparent heating (Yanai et al., 1973), which includes longwave radiation, condensation heating and divergence of eddy static energy transport. Equation (1) implies that the change of vertical motion under global warming is determined by the combined effect of the static stability and apparent heating changes. It has been shown that global warming leads to an increase of both static stability and diabatic heating. Thus, it is necessary to reveal their relative roles; in particular, how their relative effects change with height. Figure 4 illustrates how the static stability parameter and the diabatic heating change vertically. Whereas the static stability parameter increases throughout the troposphere, apparent heating exhibits a maximum increase in the upper troposphere, which is consistent with a previous study by Huang et al. (2013). The diagnosis of horizontal temperature advection shows that this term is negligible (Fig. 4b). Therefore, Eq. (1) is indeed valid in the region of interest.

To quantitatively measure the relative contributions of the static stability and diabatic heating to vertical motion change in the upper and lower troposphere, we transform Eq. (1) into the following form:

$$\Delta\omega = -\frac{1}{S}\Delta Q_1 + \frac{Q_1}{S^2}\Delta S, \quad (2)$$

where Δ represents the difference between the GW and PD state.

Figure 7 shows the diagnosis results for upper- and lower-tropospheric vertical motion based on Eq. (2). The effect of diabatic heating change exceeds (falls behind) that of static stability change above (below) 300 hPa. In other words, the strengthened upward motion in the upper troposphere is primarily caused by the diabatic heating effect, whereas the weakened upward motion in the lower troposphere is mainly

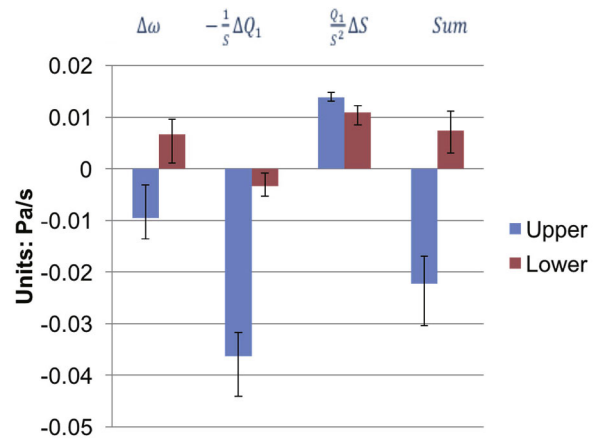


Fig. 7. The vertical p-velocity changes averaged in the upper (100–300 hPa; blue; units: Pa s^{−1}) and lower (300–1000 hPa; red) troposphere and the contributions to the vertical velocity changes by the diabatic heating term (column 2), static stability term (column 3), and sum of the two terms (column 4). All values are averaged over (2°S–2°N, 110°–130°E) based on the ensemble average of the YS, AS and KF simulations. Whiskers stand for the maximum and minimum value for each term in the YS, AS and KF simulations.

affected by enhanced atmospheric static stability. The result indicates that a more stable atmosphere does not necessarily lead to weakened vertical circulation. It is the net effect of diabatic heating and static stability changes that determines the final sign change of the vertical motion.

4. Conclusion and discussion

Idealized aqua-Planet simulations are performed with the aim to understand how the Walker circulation changes in an idealized world of no competition among monsoon circulations and no influence from excessive land warming. A zonal wavenumber-1 SST distribution is prescribed in the tropics in the PD simulation. It is found that the Walker circulation is strengthened in such an idealized world, given a uniform 2-K SST warming. Diagnosis shows that the ascending branch of the Walker cell is enhanced in the upper troposphere but weakened in the lower troposphere. As a result, a “double-cell” circulation change pattern forms, with a clockwise (anti-clockwise) circulation anomaly in the upper (lower) troposphere. The upper tropospheric circulation change dominates the strength change of the Walker circulation. The mechanism for the formation of the “double cell” circulation pattern is attributed to a greater (smaller) rate of increase of diabatic heating than static stability in the upper (lower) troposphere.

While the Walker circulation is strengthened under global warming, global average upward motion is weakened in the aqua-planet simulations (Table 3). This indicates that the global moisture budget argument put forward by Held and Soden (2006) is valid even in an idealized aqua-Planet model. It is found that global average water vapor content in the current model increases by 19% with a 2-K warming,

Table 3. The percentage change rate (GW–PD/PD) of globally averaged column-integrated moisture, upward motion, precipitation rate, net downward radiation at surface (including both longwave and shortwave radiation), and net radiative cooling in the atmosphere.

	Percentage change (%)		
	YS	AS	KF
Moisture	+19.2%	+19.5%	+18.5%
Upward motion	–8.45%	–9.90%	–6.70%
Precipitation	+3.98%	+4.57%	+4.55%
Surface radiation (downward)	+2.82%	+2.87%	+1.92%
Radiative cooling	+3.13%	+2.71%	+2.78%

whereas global mean precipitation and surface latent heat flux increase only by around 4%. The slower rate of rainfall than moisture increase is consistent with the fact that global mean ascending motion decreases in the model. Therefore, the global moisture budget argument seems to be applicable to changes of global mean upward motion, but may be insufficient to explain the change of the Walker circulation confined in the equatorial region.

The use of the traditional circulation definition implies that the major factor determining the overall strength of the Walker circulation is the zonal wind component, not vertical velocity. If the strength of the Walker circulation is defined based on maximum vertical velocity at the ascending branch of the Walker cell, one might find there is no detectable change in maximum vertical velocity in the middle troposphere under GW (see Fig. 4). If the column-integrated vertical velocity is instead used, one might find that the result is highly dependent on the area average (figure omitted).

It is worth mentioning that the traditional circulation definition depends on the upper and lower boundaries used. By examining the zonal mean zonal wind profiles, we note that the altitude of the maximum easterly (westerly) in the lower (upper) troposphere changes little between the PD and GW simulations in the current idealized aqua-planet model, even though the tropopause may increase under GW (Singh and O’Gorman, 2012). It would be interesting to examine how the upper and lower boundaries of the Walker cell might change under GW in a realistic land–sea distribution model.

The fact that the Walker circulation is strengthened in an aqua-planet simulation but weakened in the future projections of most Coupled Model Intercomparison Project Phase 5 climate models suggests that the weakening of the Walker circulation in the real world must involve factors associated with realistic land–sea distributions. We intend to investigate these factors in future work.

Acknowledgements. This study was sponsored by the China National 973 Program (Grant No. 2015CB453200), the National Natural Science Foundation of China (Grant No. 41475084), the China Scholarship Council, and the Office of Naval Research (ONR, Grant Nos. N00014-1210450 and ARCP2013-27NSY-Liu). The numerical experiments were performed on the Japan’s Earth Simulator.

The International Pacific Research Center is partially sponsored by the Japan Agency for Marine–Earth Science and Technology. This is SOEST contribution number 9475, IPRC contribution number 1130, and ESMC contribution number 056.

REFERENCES

- Arakawa, A., and W. H. Schubert, 1974: Interaction of a cumulus cloud ensemble with the large-scale environment, Part I. *J. Atmos. Sci.*, **31**, 674–701.
- Bayr, T., D. Dommenges, T. Martin, and S. B. Power, 2014: The eastward shift of the Walker Circulation in response to global warming and its relationship to ENSO variability. *Climate Dyn.*, **43**, 2747–2763, doi: 10.1007/s00382-014-2091-y.
- Clement, A. C., R. S. Seager, M. A. Cane, and S. E. Zebiak, 1996: An ocean dynamical thermostat. *J. Climate*, **9**, 2190–2196.
- Dinezio, P., A. Clement, and G. A. Vecchi, 2010: Reconciling differing views of tropical Pacific climate change. *EOS, Transactions American Geophysical Union*, **91**(16), 141–142.
- Dinezio, P. N., A. C. Clement, G. A. Vecchi, B. Soden, B. P. Kirtman, and S.-K. Lee, 2009: Climate response of the equatorial Pacific to global warming. *J. Climate*, **22**, 4873–4892.
- Endo, H., A. Kitoh, T. Ose, R. Mizuta, and S. Kusunoki, 2012: Future changes and uncertainties in Asian precipitation simulated by multiphysics and multi-sea surface temperature ensemble experiments with high-resolution Meteorological Research Institute atmospheric general circulation models (MRI-AGCMs). *J. Geophys. Res.*, **117**, D16118.
- Held, I. M., and B. J. Soden, 2006: Robust responses of the hydrological cycle to global warming. *J. Climate*, **19**, 5686–5699.
- Holton, J. R., 2004: *An Introduction to Dynamic Meteorology*. 4th ed., Academic Press, 535 pp.
- Hsu, P.-C., and T. Li, 2012: Is “rich-get-richer” valid for Indian Ocean and Atlantic ITCZ? *Geophys. Res. Lett.*, **39**, L13705, doi: 10.1029/2012GL052399.
- Huang, X. L., H. W. Chuang, A. Dessler, X. H. Chen, K. Minshwaner, Y. Ming, and V. Ramaswamy, 2013: A radiative-convective equilibrium perspective of weakening of the tropical walker circulation in response to global warming. *J. Climate*, **26**(5), 1643–1653.
- IPCC, 2007: *Climate Change 2007: The Physical Science Basis. Contribution of Working Group I to the Fourth Assessment Report of the Intergovernmental Panel on Climate Change*. Solomon, S., D. Qin, M. Manning, Z. Chen, M. Marquis, K. B. Averyt, M. Tignor, H. L. Miller, Eds., Cambridge University Press, Cambridge, United Kingdom and New York, NY, USA, 996 pp.
- IPCC, 2013: *Climate Change 2013: The Physical Science Basis. Contribution of Working Group I to the Fifth Assessment Report of the Intergovernmental Panel on Climate Change*. Stocker, T. F., and Coauthors, Eds. Cambridge University Press, Cambridge, United Kingdom and New York, NY, USA, 950 pp.
- Kain, J. S., and J. M. Fritsch, 1990: A one-dimensional entraining/detraining plume model and its application in convective parameterization. *J. Atmos. Sci.*, **47**, 2784–2802.
- Kain, J. S., and J. M. Fritsch, 1993: Convective parameterization for mesoscale models: The Kain-Fritsch scheme. *The Representation of Cumulus Convection in Numerical Models*, Emanuel and Raymond, Eds., Amer. Meteor. Soc., 165–170.
- Knutson, T. R., and S. Manabe, 1995: Time-mean response over

- the tropical Pacific to increased CO₂ in a coupled ocean-atmosphere model. *J. Climate*, **8**, 2181–2199.
- Merrifield, M. A., 2011: A shift in western Tropical Pacific Sea level trends during the 1990s. *J. Climate*, **24**, 4126–4138.
- Mizuta, R., and Coauthors, 2012: Climate simulations using the improved MRI-AGCM with 20-km grid. *J. Meteor. Soc. Japan*, **90A**, 235–260.
- Murakami, H., R. Mizuta, and E. Shindo, 2012: Future changes in tropical cyclone activity projected by multi-physics and multi-SST ensemble experiments using the 60-km-mesh MRI-AGCM. *Climate Dyn.*, **39**(9–10), 2569–2584.
- Sandeep, S., F. Stordal, P. D. Sardeshmukh, and G. P. Compo, 2014: Pacific Walker Circulation variability in coupled and uncoupled climate models. *Climate Dyn.*, **43**, 103–117, doi: 10.1007/s00382-014-2135-3.
- Schneider, T., P. A. O’Gorman, and X. J. Levine, 2010: Water vapor and the dynamics of climate changes. *Rev. Geophys.*, **48**, 302–323.
- Shine, K. P., R. G. Derwent, D. J. Wuebbles, and J.-J. Morcrette, 1990: Radiative forcing of climate. *Climate Change: The IPCC Scientific Assessment*, Houghton et al., Eds. Cambridge University Press, Cambridge, United Kingdom and New York, NY, USA, 41–68.
- Singh, M. S., and P. A. O’Gorman, 2012: Upward shift of the atmospheric general circulation under global warming: Theory and simulations. *J. Climate*, **25**(23), 8259–8276.
- Stocker, T. F., 2001: *Climate Change 2001: The Scientific Basis*. Chapter 7, J. T. Houghton, Eds., Cambridge Univ. Press, Cambridge, 417–470.
- Vecchi, G. A., and B. J. Soden, 2007: Global warming and the weakening of the tropical circulation, *J. Climate*, **20**, 4316–4340.
- Vecchi, G. A., A. Clement, and B. J. Soden, 2008: Examining the tropical Pacific’s response to global warming. *Eos, Transactions American Geophysical Union*, **89**, 81–83.
- Vecchi, G. A., B. J. Soden, A. T. Wittenberg, I. M. Held, A. Leetmaa, and M. J. Harrison, 2006: Weakening of tropical Pacific atmospheric circulation due to anthropogenic forcing. *Nature*, **441**, 73–76.
- Yanai, M., S. Esbensen, and J.-H. Chu, 1973: Determination of bulk properties of tropical cloud clusters from large-scale heat and moisture budgets. *J. Atmos. Sci.*, **30**, 611–627.
- Yoshimura, H., R. Mizuta, and H. Murakami, 2015: A spectral cumulus parameterization scheme interpolating between two convective updrafts with semi-Lagrangian calculation of transport by compensatory subsidence. *Mon. Wea. Rev.*, **143**, 597–621.
- Yukimoto, S. H., and Coauthors, 2011: Meteorological research institute-earth system model Version 1 (MRI-ESM1)—Model description. Technical Reports of the Meteorological Research Institute, No. **64**, 96 pp.
- Zhang, L., and T. Li, 2014: A simple analytical model for understanding the formation of sea surface temperature patterns under global warming. *J. Climate*, **27**, 8413–8421.